RESEARCH ARTICLE

Free vibration analysis of laminated FG-CNT reinforced composite beams using finite element method

T. VO-DUY[a,b], V. HO-HUU[a,b], T. NGUYEN-THOI[a,b*]

[a] *Division of Computational Mathematics and Engineering, Institute for Computational Science, Ton Duc Thang University, Ho Chi Minh City, Vietnam*
[b] *Faculty of Civil Engineering, Ton Duc Thang University, Ho Chi Minh City, Vietnam*
[*] Corresponding author. E-mail: nguyenthoitrung@tdt.edu.vn

ABSTRACT   In the present study, the free vibration of laminated functionally graded carbon nanotube reinforced composite beams is analyzed. The laminated beam is made of perfectly bonded carbon nanotubes reinforced composite (CNTRC) layers. In each layer, single-walled carbon nanotubes are assumed to be uniformly distributed (UD) or functionally graded (FG) distributed along the thickness direction. Effective material properties of the two-phase composites, a mixture of carbon nanotubes (CNTs) and an isotropic polymer, are calculated using the extended rule of mixture. The first-order shear deformation theory is used to formulate a governing equation for predicting free vibration of laminated functionally graded carbon nanotubes reinforced composite (FG-CNTRC) beams. The governing equation is solved by the finite element method with various boundary conditions. Several numerical tests are performed to investigate the influence of the CNTs volume fractions, CNTs distributions, CNTs orientation angles, boundary conditions, length-to-thickness ratios and the numbers of layers on the frequencies of the laminated FG-CNTRC beams. Moreover, a laminated composite beam combined by various distribution types of CNTs is also studied.

KEYWORDS   free vibration analysis, laminated FG-CNTRC beam, finite element method, first-order shear deformation theory, composite material

1   Introduction

Carbon nanotube (CNT), a new advantaged material with exceptional electronic and mechanical properties over carbon fibers [1], was considered as a newly excellent candidate for reinforcement of composite materials [2–15]. Moreover, the CNTs were successfully studied in regard to functionally graded (FG) distribution along the thickness direction [16], which significantly change the mechanical behavior of CNT reinforced composite structures. Owing to these CNT's advantages, a large number of studies have recently focused on the mechanical analysis of functionally graded carbon nanotubes reinforced composite (FG-CNTRC) structures. For example, recent works done on analysis structural behavior of FG-CNTRC structures (e.g., beams and plates) are reported in Refs. [4,17–34]. A

comprehensive review of the mechanical analysis of FG-CNTRC structures is reported by Liew et al. [35].

Due to various exceptional mechanical properties like high strength-to-weight ratio, high stiffness-to-weight ratio, superior fatigue properties, high corrosion resistance, and flexibility in design, composite beams have been widely used in aircraft structures, space vehicles, turbomachines and other engineering applications. It is well known that composite beams in these applications often operate in complex environmental conditions and are commonly exposed to a variety of dynamic excitations which may result in excessive vibration and fatigue damage [36]. Therefore, to design composite beams working effectively in these applications, the accurate knowledge of the vibration behaviors of composite beams is very importance (see, for example, some references on frequency optimization of composite structures [37–39]). Moreover, for damage assessment of composite beam

during their service life, the vibration characteristic of composite beams is really necessary [40–42]. In the last few decades, a lot of relevant papers [43–53] have fully addressed the free vibration of the traditional composite beams. Meanwhile, research works pertaining to the free vibration analysis of FG-CNTRC beams [17,22,23,34] have been developed. There still exist some issues that need to be addressed adequately, e.g., the free vibration analysis of multi-layer FG-CNTRC beams and the effect of different stacking of FG-CNTRC lamina.

This paper hence makes an effort to fulfill in the above-mentioned research gaps by studying the free vibration analysis of laminated FG-CNTRC beams. Here, it was considered that the laminated beam is composed of perfectly bonded carbon nanotubes reinforced composite (CNTRC) layers and distinct distributions of single-walled carbon nanotubes (SWCNTs) through the thickness of the layers. Concerning the effective material properties of the laminated nanocomposite beams, the extended rule of mixture is used. In order to build the system of equations ruling the beam deformation, we used the linear two-node element combined with the first-order shear deformation theory. In this work, two types of multilayered composite beams are analyzed including: (1) The multilayered with the same CNT distributions; and (2) the multilayered with various CNT distributions, and the corresponding numerical results are presented. In addition, the effects of CNT distributions, CNT volume fractions, CNT orientation angles, number of layers, length-to-thickness ratios and boundary conditions on the free vibration response of laminated FG-CNTRC beams are also illustrated.

The remainder of the paper is organized as follows. Section 2 presents material properties of the FG-CNTRC materials. Section 3 describes the finite element method for free vibration analysis of the laminated FG-CNTRC beam based on the first-order deformation theory. Section 4 examines some numerical examples. Section 5 draws some conclusions.

2 Material properties of FG-CNTRC beams

In this study, laminated composite beams composed of many layers of CNTRC materials are considered. In each layer, it is assumed that CNTs are (10,10) armchair SWCNTs and the matrix is supposed to be isotropic and homogeneous. The effective material properties of the two-phase composites, mixture of CNTs and an isotropic polymer, can be defined according to the extended rule of mixtures [16],

$$E_{11} = \eta_1 V_{CNT} E_{11}^{CNT} + V_m E_m, \qquad (1)$$

$$\frac{\eta_2}{E_{22}} = \frac{V_{CNT}}{E_{22}^{CNT}} + \frac{V_m}{E_m}, \qquad (2)$$
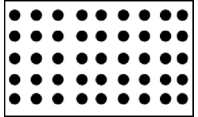
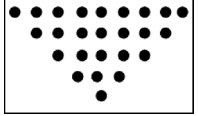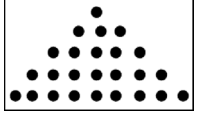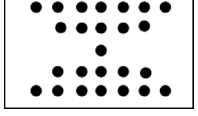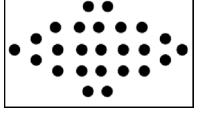$$\frac{\eta_3}{G_{12}} = \frac{V_{CNT}}{G_{12}^{CNT}} + \frac{V_m}{G_m}, \qquad (3)$$

$$v_{12} = V_{CNT} v_{12}^{CNT} + V_m v_m, \qquad (4)$$

$$\rho = V_{CNT} \rho_{CNT} + V_m \rho_m, \qquad (5)$$

where E_{11}^{CNT}, E_{22}^{CNT} and G_{12}^{CNT} are Young's moduli and shear modulus of the CNTs, E_m and G_m are Young's modulus and shear modulus of the isotropic matrix, η_1, η_2 and η_3 are CNT/matrix efficiency parameters which can be determined by matching the elastic modulus of CNTRCs observed from the molecular dynamics (MD) simulation results with the numerical ones obtained from the rule of mixture, v_{12}^{CNT} and v_m are Poisson's ratios of CNTs and matrix, respectively, ρ_{CNT} and ρ_m are mass densities of the CNTs and matrix, respectively, V_{CNT} and V_m, related by $V_{CNT} + V_m = 1$, are respectively the volume fractions for CNTs and matrix.

Currently, CNTRC materials have been developed to five distributions of CNTs along the thickness direction, including a uniformly distributed (UD) and four different FG, namely FG-V, FG-Λ, FG-X and FG-O. The volume fraction of CNTs, therefore, depends on its distribution as follows:

$$V_{CNT}(z) = V_{CNT}^* \qquad \text{UD}$$

$$V_{CNT}(z) = \left(1 + \frac{2z}{h}\right) V_{CNT}^* \qquad \text{FG-V}$$

$$V_{CNT}(z) = \left(1 - \frac{2z}{h}\right) V_{CNT}^* \qquad \text{FG-Λ}$$

$$V_{CNT}(z) = \frac{4|z|}{h} V_{CNT}^* \qquad \text{FG-X}$$

$$V_{CNT}(z) = 2\left(1 - \frac{2|z|}{h}\right) V_{CNT}^* \qquad \text{FG-O}$$

where V_{CNT}^* is the volume fraction of CNTs that is determined by

$$V_{CNT}^* = \frac{w_{CNT}}{w_{CNT} + \frac{\rho_{CNT}}{\rho_m} - \frac{\rho_{CNT}}{\rho_m} w_{CNT}}, \qquad (6)$$

in which w_{CNT} is the mass fraction of the CNTs in composite beams.

3 Free vibration of laminated FG-CNTRC beams

In the literature, many papers have been published in recent decades and many mathematical models and solution techniques have been developed for structural analysis (see, for example, Refs. [44,54–71]). In these approaches, the finite element method is one of the most popular methods because it is simple to understand and to implement. Besides, the first-order shear deformation theory (FSDT) provides a balance between computational efficiency and accuracy for the global structural behavior of thin and moderately thick composite beams. Under such circumstances, in the present work, the finite element method based on the first order shear deformation theory is used for free vibration analysis of laminated FG-CNTRC beams. More detail on the formulation of this method is presented below.

Let us consider a laminated composite beam consisting of N layers. The size of the beam is characterized by the length L, the width b and the thickness h. A global coordinate $Oxyz$ is attached at the center of the beam such that the x-axis is in the longitudinal direction, as depicted in Fig. 1. Here the bending of the beam on the yz-plane is not considered. In each layer, we denote the fiber orientation angles by $\theta^{(1)}$, $\theta^{(2)}$, $\theta^{(3)}$, ..., $\theta^{(N)}$, the fiber volume fractions by V_{CNT}^1, V_{CNT}^2, ..., V_{CNT}^N, and the vertical coordinate of layers by z_1, z_2, ..., z_N, z_{N+1}.

Based on FSDT where the influence of shear deformation and rotary inertia is considered, the displacement field of the laminated composite beam is given by

$$\begin{cases} u(x,z) = u_0 + z\beta_x(x) \\ w(x,z) = w_0(x) \end{cases}, \tag{7}$$

where u and w are x-direction and z-direction displacements of the beam, respectively, u_0 and w_0 are the x-direction and z-direction displacements of the beam neutral axis, respectively, and β_x is the rotation of the cross section.

According to Eq. (7), the strain field of the beam is expressed as follows

$$\boldsymbol{\varepsilon} = \begin{bmatrix} \varepsilon_x \\ \gamma_{xz} \end{bmatrix} = \begin{bmatrix} u_{0,x} + z\beta_{x,x} \\ w_{0,x} + \beta_x \end{bmatrix}. \tag{8}$$

If transverse normal stresses are neglected, the constitutive relations for the kth layer of the beam take the form

$$\boldsymbol{\sigma}^{(k)} = \overline{\boldsymbol{Q}}^{(k)}(z)\boldsymbol{\varepsilon}^{(k)}, \tag{9}$$

where

$$\boldsymbol{\sigma}^{(k)} = \begin{bmatrix} \sigma_x^{(k)} \\ \tau_{xz}^{(k)} \end{bmatrix}, \ \boldsymbol{\varepsilon}^{(k)} = \begin{bmatrix} \varepsilon_x^{(k)} \\ \gamma_{xz}^{(k)} \end{bmatrix},$$

$$\overline{\boldsymbol{Q}}^{(k)}(z) = \begin{bmatrix} \overline{Q}_{11}^{(k)}(z) & 0 \\ 0 & \overline{Q}_{55}^{(k)}(z) \end{bmatrix}, \tag{10}$$

where

$$\overline{Q}_{11}^{(k)}(z) = Q_{11}^{(k)}(z)\cos^4\theta^{(k)} + 2\left(Q_{12}^{(k)}(z) + 2Q_{66}^{(k)}(z)\right)$$

$$\cdot \sin^2\theta^{(k)}\cos^2\theta^{(k)} + Q_{22}^{(k)}(z)\sin^4\theta^{(k)}, \tag{11}$$

$$\overline{Q}_{55}^{(k)}(z) = Q_{44}^{(k)}(z)\sin^2\theta^{(k)} + Q_{55}^{(k)}(z)\cos^2\theta^{(k)}, \tag{12}$$

where the stiffness coefficients $Q_{ij}^{(k)}(z)$ of the kth lamina in the material coordinate system are

$$Q_{11}^{(k)}(z) = \frac{E_{11}^{(k)}(z)}{1 - v_{12}^{(k)}(z)v_{21}^{(k)}(z)},$$

$$Q_{12}^{(k)} = \frac{v_{12}^{(k)}E_{22}^{(k)}(z)}{1 - v_{12}^{(k)}(z)v_{21}^{(k)}(z)},$$

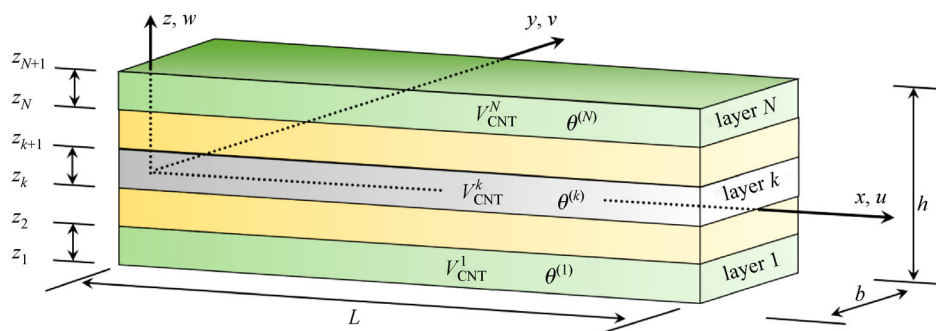**Fig. 1** Sketch of a laminated composite beam

$$Q_{22}^{(k)} = \frac{E_{22}^{(k)}(z)}{1 - v_{12}^{(k)}(z)v_{21}^{(k)}(z)},$$

$$Q_{44}^{(k)}(z) = G_{23}^{(k)}(z),$$

$$Q_{55}^{(k)}(z) = G_{13}^{(k)}(z),$$

$$Q_{66}^{(k)}(z) = G_{12}^{(k)}(z), \tag{13}$$

where $E_{11}^{(k)}$ and $E_{22}^{(k)}$ are the effective Young's moduli, $G_{12}^{(k)}$, $G_{13}^{(k)}$ and $G_{23}^{(k)}$ are the shear moduli, $v_{12}^{(k)}$ and $v_{21}^{(k)}$ are Poisson's ratios. These parameters depend on the CNT volume fraction of the kth layer. The five distributions of CNTs for the kth layer of the laminated CNTRC beam are rewritten by

$$\begin{cases} V_{\mathrm{CNT}}(z) = V_{\mathrm{CNT}}^* & \text{UD} \\[2mm] V_{\mathrm{CNT}}(z) = 2\dfrac{z - z_k}{z_{k+1} - z_k} V_{\mathrm{CNT}}^* & \text{FG-V} \\[2mm] V_{\mathrm{CNT}}(z) = -2\dfrac{z - z_{k+1}}{z_{k+1} - z_k} V_{\mathrm{CNT}}^* & \text{FG-}\Lambda \\[2mm] V_{\mathrm{CNT}}(z) = 4\dfrac{\left|z - \dfrac{z_{k+1} + z_k}{2}\right|}{z_{k+1} - z_k} V_{\mathrm{CNT}}^* & \text{FG-X} \\[2mm] V_{\mathrm{CNT}}(z) = \left(2 - 4\dfrac{\left|z - \dfrac{z_{k+1} + z_k}{2}\right|}{z_{k+1} - z_k}\right) V_{\mathrm{CNT}}^* & \text{FG-O} \end{cases} \tag{14}$$

The governing equation for free vibration of the laminated composite beam can be obtained by using the Hamilton's principle

$$\delta \int_{t_0}^{t_1} \left[\frac{1}{2} \int_V (\boldsymbol{\sigma}^{(k)})^{\mathrm{T}} \boldsymbol{\varepsilon}^{(k)} \mathrm{d}V - \frac{1}{2} \int_V \rho^{(k)} (\dot{u}^2 + \dot{w}^2) \mathrm{d}V \right] \mathrm{d}t = 0, \tag{15}$$

where δ is the notation of variation operator, $\rho^{(k)}$ is the mass density of the kth layer and the over-dot represents a partial derivative with respect to time t.

Then the Galerkin weak form of free vibration analysis of the laminated composite beam is given by

$$\int_L \delta(\Lambda \boldsymbol{u})^{\mathrm{T}} \boldsymbol{D}(\Lambda \boldsymbol{u}) \mathrm{d}x + \int_L \delta \boldsymbol{u}^{\mathrm{T}} \boldsymbol{m} \ddot{\boldsymbol{u}} \mathrm{d}x = 0, \tag{16}$$

where

$$\boldsymbol{\Lambda} = \begin{bmatrix} \dfrac{\partial}{\partial x} & 0 & 0 \\[2mm] 0 & 0 & \dfrac{\partial}{\partial x} \\[2mm] 0 & \dfrac{\partial}{\partial x} & 1 \end{bmatrix}, \quad \boldsymbol{u} = \begin{bmatrix} u_0 \\ w_0 \\ \beta_x \end{bmatrix}, \tag{17}$$

and $\ddot{\boldsymbol{u}}$ is the second-order derivative with respect to time of $\boldsymbol{u}$. The formulas for $\boldsymbol{D}$ and $\boldsymbol{m}$ are expressed as follows:

$$\boldsymbol{D} = \begin{bmatrix} A_{11} & B_{11} & 0 \\ B_{11} & D_{11} & 0 \\ 0 & 0 & \kappa A_{55} \end{bmatrix}, \quad \boldsymbol{m} = \begin{bmatrix} I_0 & 0 & I_1 \\ 0 & I_0 & 0 \\ I_1 & 0 & I_2 \end{bmatrix}, \tag{18}$$

where $\kappa = 5/6$ is the shear correction factor and $A_{11}, B_{11}, D_{11}, A_{55}, I_0, I_1, I_2$ are defined by

$$(A_{11}, B_{11}, D_{11}) = b \sum_{k=1}^{nL} \int_{z_k}^{z_{k+1}} \overline{Q}_{11}^{(k)}(z)(1, z, z^2) \mathrm{d}z,$$

$$A_{55} = b \sum_{k=1}^{nL} \int_{z_k}^{z_{k+1}} \overline{Q}_{55}^{(k)}(z) \mathrm{d}z,$$

$$(I_0, I_1, I_2) = b \sum_{k=1}^{nL} \int_{z_k}^{z_{k+1}} \rho^{(k)}(z)(1, z, z^2) \mathrm{d}z. \tag{19}$$

By using finite element method, the beam is divided into Ne elements and each element has two nodes. On each element, the displacement field of the beam, $\boldsymbol{u}^e$, is approximated by linear shape functions in the natural coordinate, $N_1^e(\xi) = \frac{1}{2}(1 - \xi)$ and $N_2^e(\xi) = \frac{1}{2}(1 + \xi)$, as follows:

$$\boldsymbol{u}^e = \boldsymbol{N}^e \boldsymbol{d}^e, \tag{20}$$

in which $\boldsymbol{d}^e = [\,u_{01} \quad w_{01} \quad \beta_{x1} \quad u_{02} \quad w_{02} \quad \beta_{x2}\,]^{\mathrm{T}}$ is the nodal displacement vector of element e and

$$\boldsymbol{N}^e = \begin{bmatrix} N_1^e & 0 & 0 & N_2^e & 0 & 0 \\ 0 & N_1^e & 0 & 0 & N_2^e & 0 \\ 0 & 0 & N_1^e & 0 & 0 & N_2^e \end{bmatrix}. \tag{21}$$

After substituting Eq. (20) into Eq. (16), the discrete equation for free vibration analysis of the laminated composite beam is represented by

$$\boldsymbol{M}\ddot{\boldsymbol{d}} + \boldsymbol{K}\boldsymbol{d} = 0, \tag{22}$$

where $\boldsymbol{d}$ is the displacement vector, $\ddot{\boldsymbol{d}}$ is the second-order derivative with respect to time of the displacement, $\boldsymbol{M}$ and $\boldsymbol{K}$ are the global mass matrix and stiffness matrix which are

the assemblies of elemental ones and given by

$$
\begin{cases}
\boldsymbol{K} = \sum_{e=1}^{Ne} \boldsymbol{K}^e = \sum_{e=1}^{Ne} \int_{-1}^{1} (\boldsymbol{B}^e)^{\mathrm{T}} \boldsymbol{D} \boldsymbol{B}^e \frac{l^e}{2} \mathrm{d}\xi \\
\boldsymbol{M} = \sum_{e=1}^{Ne} \boldsymbol{M}^e = \sum_{e=1}^{Ne} \int_{-1}^{1} (\boldsymbol{N}^e)^{\mathrm{T}} \boldsymbol{m} \boldsymbol{N}^e \frac{l^e}{2} \mathrm{d}\xi
\end{cases}, \quad (23)
$$

where l^e is the length of the eth element and $\boldsymbol{B}^e$ is defined by

$$
\boldsymbol{B}^e = \begin{bmatrix}
N_{1,\xi}^e \left(\frac{2}{l^e}\right) & 0 & 0 & N_{2,\xi}^e \left(\frac{2}{l^e}\right) & 0 & 0 \\
0 & 0 & N_{1,\xi}^e \left(\frac{2}{l^e}\right) & 0 & 0 & N_{2,\xi}^e \left(\frac{2}{l^e}\right) \\
0 & N_{1,\xi}^e \left(\frac{2}{l^e}\right) & N_1^e & 0 & N_{2,\xi}^e \left(\frac{2}{l^e}\right) & N_2^e
\end{bmatrix}. \quad (24)
$$

To ensure the well-behaved element performance that is devoid of shear locking in slender beams, a selective reduced integration scheme [72,73] is used. The idea of the reduced integration scheme is to split the strain energy into two parts: The bending-related term and the shear-related one. Two different integration rules are then used, respectively, for the bending strain energy and the shear strain energy. In this study, a single Gaussian point is used for calculating the bending stiffness (with respect to the bending strain energy) and transverse shear stiffness (with respect to shear strain energy). More detail on this technique, interesting readers can refer to Refs. [72,73].

The natural frequency (ω) and mode shape (ϕ) of the beam are obtained by solving the eigenvalue problem which is derived from Eq. (22) as follows

$$
(\boldsymbol{K} - \omega^2 \boldsymbol{M})\phi = 0. \quad (25)
$$

The support conditions for clamped (C), hinged (H) and free (F) at the ends $x = 0, L$ are

$$
\begin{cases}
\text{C} & u_0 = w_0 = \beta_x = 0 \\
\text{H} & u_0 = w_0 = 0 \\
\text{F} & \text{no contraints}
\end{cases}. \quad (26)
$$

It should be mentioned that in the previous work by Lin and Xiang [34], they analyzed the free vibration of FG-CNT beams. However, this study only limited to single layer-FG-CNTRC beams. Therefore, their finite element formulation is simpler than the present formulation while the effects of CNT orientation angles (Eq. (10)) and the change of CNT distributions in each layer (as in Eq. (14)) are neglected in their work.

4 Numerical examples

4.1 Comparison study

As mentioned before, to the best of our knowledge there is no work reported on free vibration analysis of laminated FG-CNTRC beams. Therefore, to assure the validity of free vibration analysis for single-layer FG-CNTRC beams and multilayered composite beams, two comparison studies are given in this section.

For the first comparison study, the fundamental frequency parameter of a single layer FG-CNTRC beam is evaluated and compared with the results of Yas and Samadi [2] using the generalized differential quadrature method (GDQM) and Lin and Xiang [34] using the p-Ritz method. The material properties of the FG-CNTRC beam at room temperature (300 K) are the same as those used in study of Yas and Samadi [2] in which poly methyl methacrylate, referred to PMMA, is considered as the matrix and the armchair (10,10) SWCNTs are selected as reinforcements. Details of the parameters are listed in Table 1. It is also assumed that $G_{23}^{(k)}(z) = G_{13}^{(k)}(z) = G_{12}^{(k)}(z)$ and $v_{21}^{(k)}(z) = v_{12}^{(k)}(z)$. Three different values of CNTs volume fraction and their corresponding CNT/matrix efficiency parameters are given as follows: $V_{\mathrm{CNT}}^* = 0.12$, $\eta_1 = 1.2833$ and $\eta_2 = 1.0556$; $V_{\mathrm{CNT}}^* = 0.17$, $\eta_1 = 1.3414$ and $\eta_2 = 1.7101$; and $V_{\mathrm{CNT}}^* = 0.28$, $\eta_1 = 1.3238$ and $\eta_2 = 1.7380$. In addition, it is assumed that $\eta_3 = \eta_2$. The beam for length to thickness ratio (L/h) of 15 is divided into 32 elements equal of lengths for finite element analysis. The obtained dimensionless frequencies with various CNT volume fractions, boundary conditions and types of distributions are provided in Tables 2 and 3. It can be seen that the present results are in good agreement with those solved in Refs. [2,34]. This result demonstrates the reliability of the finite element analysis for the FG-CNTRCs beams.

For the second comparison study, the dimensionless

Table 1 Material parameters of a FG-CNTRC beam

parameters (unit)	matrix	fiber
Poisson's coefficient	$v_{\mathrm{m}} = 0.3$	$v_{12}^{\mathrm{CNT}} = 0.19$
mass density (kg/m³)	$\rho_{\mathrm{m}} = 1190$	$\rho_{\mathrm{CNT}} = 17.2$
Young's modulus (GPa)	$E_{\mathrm{m}} = 2.5$	$E_{11}^{\mathrm{CNT}} = 600$, $E_{22}^{\mathrm{CNT}} = 600$
shear modulus (GPa)	–	$G_{12}^{\mathrm{CNT}} = 10$

Table 2 Comparison of dimensionless frequency parameters, $\bar{\omega} = \omega \dfrac{L^2}{h} \sqrt{\dfrac{\rho_m}{E_m}}$ of FG-CNTRC beams for $V_{CNT}^* = 0.12$ and 0.17

V_{CNT}^*	BC	mode	FG-X		UD		FG-V		FG-O	
			FEM (present)	GDQM [2]	FEM (present)	GDQM [2]	FEM (present)	GDQM [2]	FEM (present)	GDQM [2]
0.12	CC	1	1.5953	1.6000	1.5052	1.5085	1.4046	1.4068	1.3166	1.3180
		2	3.2568	3.2629	3.1317	3.1353	2.9980	2.9997	2.8763	2.8762
		3	5.1517	5.1514	5.0022	4.9979	4.8433	4.8363	4.6940	4.6840
	CH	1	1.3547	1.3577	1.2426	1.2444	1.1518	1.1529	1.0327	1.0331
		2	3.1768	3.1817	3.0137	3.0159	2.8468	2.8472	2.6827	2.6814
		3	5.1103	5.1092	4.9393	4.9342	4.7556	4.7474	4.5731	4.5619
	HH	1	1.1139	1.1150	0.9748	0.9753	0.9451	0.9453	0.7529	0.7527
		2	3.0780	3.0814	2.8722	2.8728	2.6436	2.6424	2.4588	2.4562
		3	5.0713	5.0695	4.8765	4.8704	4.6768	4.6675	4.4445	4.4320
	CF	1	0.4411	0.4416	0.3761	0.3764	0.3192	0.3193	0.2808	0.2809
		2	1.8461	1.8497	1.6984	1.7006	1.5460	1.5473	1.4260	1.4266
		3	3.8743	3.8777	3.6643	3.6648	3.4393	3.4380	3.2519	3.2489
0.17	CC	1	2.0409	2.0498	1.9083	1.9144	1.7677	1.7721	1.6471	1.6500
		2	4.1962	4.2111	4.0088	4.0187	3.8242	3.8312	3.6527	3.6565
		3	6.6638	6.6753	6.4310	6.4348	6.2143	6.2139	6.0025	5.9970
	CH	1	1.7131	1.7188	1.5567	1.5602	1.4321	1.4344	1.2757	1.2769
		2	4.0718	4.0843	3.8328	3.8402	3.6020	3.6064	3.3758	3.3772
		3	6.5991	6.6094	6.3347	6.3370	6.0789	6.0765	5.8204	5.8126
	HH	1	1.3808	1.3830	1.1989	1.1999	1.1601	1.1609	0.9155	0.9155
		2	3.9201	3.9293	3.6235	3.6276	3.3075	3.3084	3.0591	3.0577
		3	6.5365	6.5447	6.2367	6.2363	5.9550	5.9498	5.6247	5.6139
	CF	1	0.5406	0.5413	0.4583	0.4587	0.3863	0.3866	0.3393	0.3394
		2	2.3364	2.3437	2.1319	2.1365	1.9258	1.9287	1.7669	1.7685
		3	4.9590	4.9706	4.6554	4.6614	4.3471	4.3500	4.0915	4.0913

*Note: BC = boundary condition

Table 3 Comparison of dimensionless frequency parameters, $\bar{\omega} = \omega \dfrac{L^2}{h} \sqrt{\dfrac{\rho_m}{E_m}}$ of FG-CNTRC beams for $V_{CNT}^* = 0.28$

BC	mode	FG-X			FG-UD			FG-Λ		
		FEM (present)	GDQM [2]	p-Ritz [34]	FEM (present)	GDQM [2]	p-Ritz [34]	FEM (present)	GDQM [2]	p-Ritz [34]
HH	1	1.6423	1.6493	1.6409	1.4362	1.4401	1.4348	1.3990	1.4027	1.3975
	2	4.4443	4.4752	4.4333	4.1162	4.1362	4.1050	3.8487	3.8639	3.8370
	3	7.2596	7.3068	7.2258	6.8940	6.9245	6.8595	6.7349	6.7618	6.6976
CF	1	0.6566	0.6586	0.6566	0.5601	0.5612	0.5600	0.4754	0.4761	0.4753
	2	2.6797	2.6987	2.6763	2.4482	2.4614	2.4449	2.2578	2.2685	2.2543
	3	5.5759	5.6150	5.5589	5.2175	5.2446	5.2005	4.9767	5.0007	4.9590

frequency of a four-layered angle-ply [θ/–θ/–θ/θ] beam with four different types of boundary conditions and various CNTs orientation angles is calculated from the present approach, and the obtained results are compared with those by Chandrashekhara et al. [43] and Nguyen et al. [50]. The beam is made of AS/3501-6 graphite-epoxy materials whose properties are used the same as in Refs. [43,50]. For finite element analysis, the beam is divided into 32 elements equally. The frequencies for ratio $L/h = 15$ of the present study and the reference are shown in Table 4. It can be observed that the difference between the results is very small.

Table 4   Comparison of dimensionless frequency parameter $\overline{\omega} = \omega \dfrac{L^2}{h}\sqrt{\dfrac{\rho}{E_{11}}}$ of four-layered angle-ply $[\theta/-\theta/-\theta/\theta]$ beams

BC	method	frequency						
		0°	15°	30°	45°	60°	75°	90°
CF	FSDT [43]	0.9820	0.9249	0.7678	0.5551	0.3631	0.2723	0.2619
	HSDT [50]	0.9832	0.9259	0.7683	0.5553	0.3631	0.2722	0.2618
	present	0.9821	0.925	0.7679	0.5552	0.3632	0.2724	0.2619
HH	FSDT [43]	2.6560	2.5105	2.1032	1.5368	1.0124	0.7611	0.7320
	HSDT [50]	2.6563	2.5108	2.1033	1.5367	1.0121	0.7608	0.7317
	present	2.6589	2.5133	2.1056	1.5386	1.0136	0.7620	0.7329
CH	FSDT [43]	3.7305	3.5593	3.0573	2.3032	1.5511	1.1753	1.1312
	present	3.7362	3.565	3.0625	2.3075	1.5541	1.1776	1.1335
CC	FSDT [43]	4.8487	4.6635	4.0981	3.1843	2.1984	1.6815	1.6200
	HSDT [50]	4.9116	4.7173	4.1307	3.1973	2.2019	1.6825	1.6205
	present	4.8577	4.6725	4.1069	3.1922	2.2045	1.6862	1.6244

* Note: FSDT: First-order shear deformation theory; HSDT: Higher-order shear deformation theory

4.2   Parametric study

After performing comparison studies, parametric studies are done in this section to analyze the influences of involved parameters on the free vibration of a laminated FG-CNTRC beam. In this study, the material and geometrical parameters of the beam are the same as in the first comparison study of the previous examples. It should be noted that the length-to-thickness ratio is chosen to be 15 for all examinations except for the case of examination the effect of length-to-thickness ratio on the frequencies.

Table 5 presents the dimensionless frequencies of the cross-ply $[0°/90°]$ FG-CNTRC beams for the case of V^*_{CNT} = 0.12 with different boundary conditions. It can be seen that the trend of frequency looks very similar to the case of

Table 5   First three dimensionless frequencies of cross-ply $[0°/90°]$ FG-CNTRC beams

BC	mode	FG-X	UD	FG-V	FG-O
CC	1	1.0433	0.9373	0.8185	0.7923
	2	2.4475	2.2568	2.0305	1.9750
	3	4.1450	3.8868	3.5747	3.4902
CH	1	0.8319	0.7506	0.6294	0.6443
	2	2.2198	2.0285	1.7828	1.7613
	3	3.9548	3.6757	3.3259	3.2623
HH	1	0.7117	0.6576	0.5191	0.5850
	2	1.8890	1.6831	1.4651	1.4086
	3	3.8043	3.5198	3.1156	3.1153
CF	1	0.1939	0.1679	0.1415	0.1361
	2	1.0830	0.9614	0.8306	0.8011
	3	2.6458	2.4040	2.1320	2.0635

only one layer, as shown in Table 2, i.e., the FG-X, UD, FG-V and FG-O beams have decreasing frequency, respectively for all boundary conditions. In this case, however, there is a small difference when the first frequency of the FG-O beam is greater than that of the FG-V beam for boundary conditions of CH and HH.

Table 6 shows the dimensionless frequencies of the cross-ply $[0°/90°/0°]$ FG-CNTRC beams for the case of V^*_{CNT} = 0.12 with different boundary conditions. Similar to the results in Table 2, the FG-X beam yields the largest frequency while the FG-O beam has the smallest frequency for all boundary conditions.

Tables 7–10 provide the dimensionless frequency of four-layered angle-ply $[\theta/-\theta/-\theta/\theta]$ FG-CNTRC beams for the case of V^*_{CNT} = 0.12 with various CNTs orientation angles and different types of boundary conditions. In addition, the effect of CNTs orientation angle on frequency for other cases of CNT volume fraction is also performed and illustrated in Fig. 2 where the FG-X beam with boundary condition of CC is examined. As can be observed, the frequency decreases as the CNTs orientation angle θ decreases from 90° to 0° for all distributions of CNT, boundary conditions and for three values of CNTs volume fraction.

Figure 3 shows the dimensionless frequency of the angle-ply $[45°/-45°/-45°/45°]$ FG-CNTRC beam with different distributions and boundary conditions for the case of V^*_{CNT} = 0.17. It can be seen from the figure that the frequencies of FG-X beam are the largest; however, the difference of frequencies between FG-X beam and the other beams is small for all boundary conditions.

Figure 4 shows the dimensionless frequency of the angle-ply $[45°/-45°/-45°/45°]$ FG-X beam with clamped-clamped boundary condition and various length-to-thickness ratios. As can be seen from Fig. 4, the dimensionless

Table 6 First three dimensionless frequencies of a cross-ply [0°/90°/0°] FG-CNTRC beams

BC	mode	FG-X	UD	FG-V	FG-O
CC	1	1.5074	1.4961	1.4920	1.4885
	2	3.1376	3.1195	3.1170	3.1123
	3	5.0127	4.9876	4.9880	4.9824
CH	1	1.2436	1.2317	1.2269	1.2211
	2	3.0184	2.9976	2.9917	2.9850
	3	4.9491	4.9223	4.9205	4.9137
HH	1	0.9747	0.9621	0.9602	0.9486
	2	2.8755	2.8516	2.8406	2.8330
	3	4.8856	4.8567	4.8532	4.8443
CF	1	0.3758	0.3703	0.3663	0.3642
	2	1.6999	1.6842	1.6760	1.6707
	3	3.6698	3.6437	3.6350	3.6273

Fig. 2 The first dimensionless frequency of angle-ply [$\theta/-\theta/-\theta/\theta$] FG-X beam with boundary condition of CC

Fig. 3 The first dimensionless frequency of the angle-ply [45°/−45°/−45°/45°] FG-CNTRC beam with various distributions and boundary conditions for the case of $V_{CNT}^* = 0.17$
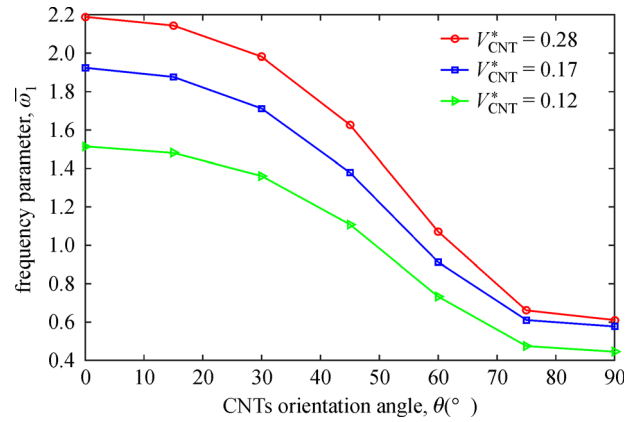
frequency of the beam is reduced when the length-to-thickness ratio increases.

Table 11 shows the dimensionless frequency of a laminated FG-CNTRC beam for the case of $V_{CNT}^* = 0.12$ with various types of distributions, boundary conditions and numbers of layers. The CNTs orientation angle of each lamina is 0°. It is seen from Table 11 that when the number of layers increases the frequency of the FG-V and FG-O beams increase while that of the FG-X beam decreases. Moreover, the frequency of these beams converges to that of the UD beam. The illustration of this comment can be seen in Fig. 5 that depicts the first dimensionless frequency of these beams for the boundary condition of CC.
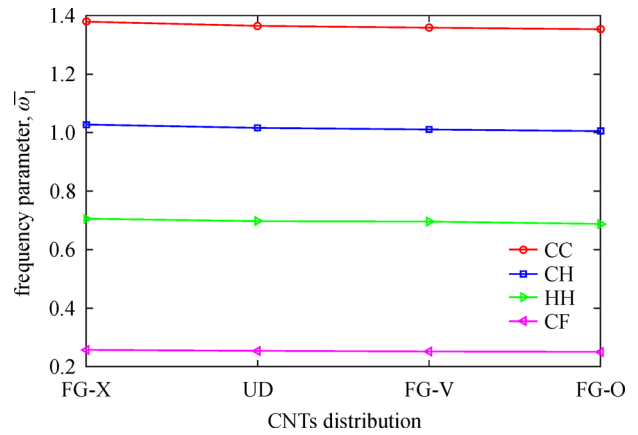
Table 12 lists the dimensionless frequency of the three-layered [0°/0°/0°] beams that are combined by different types of CNTs distributions for the case of $V_{CNT}^* = 0.12$.

Table 7 First three dimensionless frequencies of four-layered angle-ply [$\theta/-\theta/-\theta/\theta$] FG-X beam

BC	mode	frequency						
		0°	15°	30°	45°	60°	75°	90°
CC	1	1.5147	1.4807	1.3610	1.1086	0.7332	0.4749	0.4454
	2	3.1475	3.1019	2.9388	2.5600	1.8553	1.2603	1.1870
	3	5.0244	4.9699	4.7711	4.2954	3.3204	2.3617	2.2349
CH	1	1.2525	1.2120	1.0789	0.8336	0.5235	0.3319	0.3107
	2	3.0315	2.9713	2.7608	2.3090	1.5833	1.0442	0.9807
	3	4.9628	4.8990	4.6644	4.1056	3.0377	2.0942	1.9753
HH	1	0.9851	0.9382	0.7976	0.5782	0.3452	0.2149	0.2009
	2	2.8921	2.8156	2.5534	2.0319	1.3121	0.8413	0.7883
	3	4.9015	4.8272	4.5520	3.8996	2.7437	1.8317	1.7223
CF	1	0.3806	0.3596	0.2992	0.2115	0.1241	0.0768	0.0718
	2	1.7115	1.6589	1.4862	1.1628	0.7394	0.4711	0.4412
	3	3.6864	3.6100	3.3476	2.8006	1.9308	1.2780	1.2008

Table 8 First three dimensionless frequencies of four-layered angle-ply $[\theta/-\theta/-\theta/\theta]$ UD-CNTRC beam

BC	mode	frequency						
		0°	15°	30°	45°	60°	75°	90°
CC	1	1.5052	1.4710	1.3507	1.0985	0.7265	0.4729	0.4441
	2	3.1317	3.0858	2.9216	2.5414	1.8402	1.2550	1.1836
	3	5.0022	4.9471	4.7468	4.2687	3.2962	2.3521	2.2283
CH	1	1.2426	1.2021	1.0690	0.8250	0.5185	0.3305	0.3098
	2	3.0137	2.9532	2.7417	2.2897	1.5695	1.0397	0.9778
	3	4.9393	4.8749	4.6383	4.0771	3.0139	2.0855	1.9695
HH	1	0.9748	0.9282	0.7886	0.5715	0.3417	0.2139	0.2003
	2	2.8722	2.7952	2.5323	2.0122	1.2998	0.8377	0.7859
	3	4.8765	4.8015	4.5238	3.8692	2.7203	1.8239	1.7172
CF	1	0.3761	0.3553	0.2956	0.2090	0.1229	0.0765	0.0716
	2	1.6984	1.6457	1.4731	1.1511	0.7324	0.4691	0.4399
	3	3.6643	3.5874	3.3242	2.7773	1.9140	1.2726	1.1973
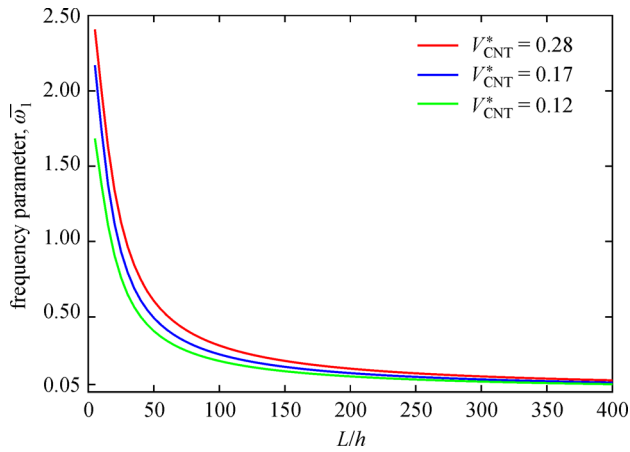
Fig. 4 The first dimensionless frequency of angle-ply $[45°/-45°/-45°/45°]$ FG-X beam with boundary condition of CC versus various length-to-thickness ratios

The combined beams are named by joining the letter of distributions of each layer. For examples, UD-X-UD means that the first and third layers have uniform distributions and the second layer has FG-X distribution. From the results in Table 12, it can be recognized that the Λ-X-V beam yields the largest frequency while the V-X-V beam produces the smallest frequency in comparison with X-UD-X and X-V-X beams. Also, the frequency of the X-UD-X and X-V-X beams is nearly the same. It can also be seen that the frequency of these combined beams is higher than that of the initial UD-UD-UD and V-V-V beams for all boundary conditions.

5   Conclusions

The paper presents the free vibration analysis of laminated

Table 9 First three dimensionless frequencies of four-layered angle-ply $[\theta/-\theta/-\theta/\theta]$ FG-V beam

BC	mode	frequency						
		0°	15°	30°	45°	60°	75°	90°
CC	1	1.5024	1.4677	1.346	1.0928	0.7235	0.4733	0.4448
	2	3.1309	3.0843	2.9177	2.5339	1.8345	1.2564	1.1855
	3	5.0047	4.9487	4.7451	4.2618	3.2890	2.3550	2.2322
CH	1	1.2390	1.1981	1.0642	0.8203	0.5164	0.3308	0.3103
	2	3.0100	2.9486	2.7348	2.2803	1.5638	1.0408	0.9794
	3	4.9400	4.8743	4.6339	4.0670	3.0053	2.0879	1.9729
HH	1	0.9733	0.9266	0.7870	0.5703	0.3413	0.2142	0.2006
	2	2.8641	2.7862	2.5209	2.0001	1.2939	0.8385	0.7872
	3	4.8757	4.7992	4.5170	3.8566	2.7116	1.8259	1.7201
CF	1	0.3727	0.3520	0.2928	0.2071	0.1222	0.0766	0.0717
	2	1.6921	1.6391	1.4656	1.1438	0.7291	0.4695	0.4406
	3	3.6584	3.5807	3.3149	2.7655	1.9069	1.2739	1.1992

Table 10 First three dimensionless frequencies of four-layered angle-ply [θ/–θ/–θ/θ] FG-O beam

BC	mode	frequency						
		0°	15°	30°	45°	60°	75°	90°
CC	1	1.4997	1.4647	1.3425	1.0888	0.7199	0.4721	0.4442
	2	3.1273	3.0804	2.9129	2.5273	1.8269	1.2534	1.1841
	3	5.0004	4.9440	4.7392	4.2533	3.2775	2.3498	2.2297
CH	1	1.2344	1.1934	1.0594	0.8158	0.5133	0.3299	0.3098
	2	3.0048	2.9431	2.7283	2.2724	1.5563	1.0381	0.9782
	3	4.9347	4.8686	4.6267	4.0570	2.9935	2.0829	1.9705
HH	1	0.9639	0.9174	0.7785	0.5638	0.3381	0.2135	0.2003
	2	2.8581	2.7799	2.5137	1.9924	1.2875	0.8362	0.7861
	3	4.8688	4.7917	4.5075	3.8440	2.6988	1.8213	1.7179
CF	1	0.3710	0.3504	0.2913	0.2060	0.1215	0.0763	0.0716
	2	1.6879	1.6348	1.4609	1.1390	0.7252	0.4683	0.4400
	3	3.6524	3.5744	3.3076	2.7568	1.8982	1.2707	1.1977

Table 11 First three dimensionless frequencies of a beam with various numbers of layers

distribution	BC	mode	2 layers	3 layers	5 layers	10 layers
FG-X	CC	1	1.5349	1.5202	1.5121	1.5086
		2	3.1746	3.1549	3.1440	3.1392
		3	5.0565	5.0332	5.0203	5.0146
	CH	1	1.2772	1.2591	1.2493	1.2451
		2	3.0675	3.0413	3.0269	3.0206
		3	5.0002	4.9730	4.9580	4.9514
	HH	1	1.0148	0.9930	0.9814	0.9764
		2	2.9381	2.9046	2.8862	2.8782
		3	4.9448	4.9133	4.8958	4.8882
	CF	1	0.3942	0.3842	0.3789	0.3766
		2	1.7437	1.7201	1.7074	1.7018
		3	3.7325	3.6989	3.6805	3.6725
FG-V	CC	1	1.4866	1.4984	1.5042	1.5066
		2	3.1095	3.1256	3.1334	3.1366
		3	4.9790	4.9983	5.0076	5.0114
	CH	1	1.2243	1.2353	1.2407	1.2429
		2	2.9832	3.0033	3.0131	3.0171
		3	4.9107	4.9327	4.9433	4.9477
	HH	1	0.9689	0.9722	0.9738	0.9745
		2	2.8279	2.8551	2.8683	2.8737
		3	4.8439	4.8677	4.8793	4.8840
	CF	1	0.3630	0.3702	0.3739	0.3754
		2	1.6675	1.6859	1.6949	1.6987
		3	3.6224	3.6494	3.6626	3.6680

(*Continued*)

distribution	BC	mode	2 layers	3 layers	5 layers	10 layers
FG-O	CC	1	1.4742	1.4934	1.5025	1.5062
		2	3.0932	3.1189	3.1311	3.1360
		3	4.9594	4.9903	5.0049	5.0108
	CH	1	1.2044	1.2270	1.2378	1.2422
		2	2.9598	2.9937	3.0098	3.0163
		3	4.8867	4.9230	4.9400	4.9469
	HH	1	0.9297	0.9553	0.9678	0.9730
		2	2.8011	2.8441	2.8645	2.8728
		3	4.8128	4.8552	4.8749	4.8830
	CF	1	0.3558	0.3672	0.3728	0.3751
		2	1.6490	1.6783	1.6923	1.6980
		3	3.5955	3.6384	3.6588	3.6671

functionally graded carbon nanotube reinforced composite beams. Here, it was considered that the laminated beam is composed of perfectly bonded CNTRC layers and distinct distributions of SWCNTs through the thickness of the layers. In order to build the system of equations ruling the beam deformation, the linear two-node element combined with the first-order shear deformation theory is used. The influence of the CNTs volume fractions, CNTs distributions, CNTs orientation angles, boundary conditions, the numbers of layers and length-to-thickness ratios on the free vibration of a laminated FG-CNTRC beam is investigated. Moreover, a laminated composite beam combined by various CNTs distributions is also studied. The numerical results indicate that

Table 12 First three dimensionless frequencies of laminated FG-CNTRC beams with various distributions of layers

BC	mode	UD-X-UD	X-UD-X	V-X-V	X-V-X	Λ-X-V
CC	1	1.5105	1.5151	1.5079	1.5151	1.5688
	2	3.1398	3.1470	3.1384	3.1480	3.2206
	3	5.0129	5.0227	5.0135	5.0250	5.1102
CH	1	1.2484	1.2535	1.2453	1.2532	1.3201
	2	3.0234	3.0319	3.0197	3.0323	3.1286
	3	4.9511	4.9617	4.9503	4.9636	5.0624
HH	1	0.9812	0.9868	0.9798	0.9867	1.0685
	2	2.8836	2.8936	2.8767	2.8930	3.0163
	3	4.8894	4.9009	4.8875	4.9025	5.0165
CF	1	0.3789	0.3814	0.3762	0.3808	0.4193
	2	1.7061	1.7127	1.7008	1.7121	1.8000
	3	3.6764	3.6871	3.6710	3.6873	3.8114
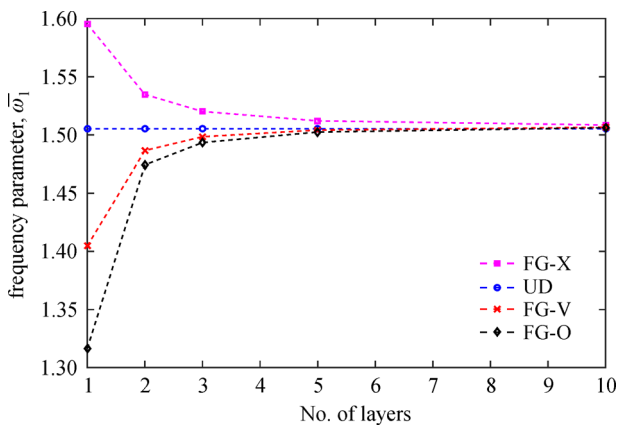
Fig. 5 First dimensionless frequencies of the clamped-clamped FG-CNTRC beams with various numbers of layers for the case of $V_{CNT}^* = 0.12$

i) The FG-X distribution yields the largest frequency while the FG-O distribution yields the smallest frequency of laminated FG-CNTRC beams.

ii) The CNT orientation angle of 0° for each layer yields the largest frequency of the laminated FG-CNTRC beams.

iii) When the number of layers increases, the frequency of FG-X distribution decreases while the frequency of the FG-V and FG-O increases. In addition, the frequencies of other CNT distributions tend to approach to the frequency of the UD distribution.

iv) The stacking sequence of CNT distributions has little influence on the frequency of the FG-CNTRC beams. Also, the stacking sequence of FG-Λ-X-V gives the largest frequencies.

v) Boundary conditions, CNT volume fractions and length-to-thickness ratios strongly effect on the frequency of laminated FG-CNTRC beams.

References

1. Sun C H, Li F, Cheng H M, Lu G Q. Axial Young's modulus prediction of single-walled carbon nanotube arrays with diameters from nanometer to meter scales. Applied Physics Letters, 2005, 87 (19): 193101

2. Yas M H, Samadi N. Free vibrations and buckling analysis of carbon nanotube-reinforced composite Timoshenko beams on elastic foundation. International Journal of Pressure Vessels and Piping, 2012, 98: 119–128

3. Jedari Salami S. Extended high order sandwich panel theory for bending analysis of sandwich beams with carbon nanotube reinforced face sheets. Physica E, Low-Dimensional Systems and Nanostructures, 2016, 76: 187–197

4. Lei Z X, Zhang L W, Liew K M. Analysis of laminated CNT reinforced functionally graded plates using the element-free kp-Ritz method. Composites. Part B, Engineering, 2016, 84: 211–221

5. Zhang L W, Song Z G, Liew K M. Optimal shape control of CNT reinforced functionally graded composite plates using piezoelectric patches. Composites. Part B, Engineering, 2016, 85: 140–149

6. Ghasemi H, Brighenti R, Zhuang X, Muthu J, Rabczuk T. Optimization of fiber distribution in fiber reinforced composite by using NURBS functions. Computational Materials Science, 2014, 83: 463–473

7. Silani M, Ziaei-Rad S, Talebi H, Rabczuk T. A semi-concurrent multiscale approach for modeling damage in nanocomposites. Theoretical and Applied Fracture Mechanics, 2014, 74: 30–38

8. Ghasemi H, Brighenti R, Zhuang X, Muthu J, Rabczuk T. Optimal fiber content and distribution in fiber-reinforced solids using a reliability and NURBS based sequential optimization approach. Structural and Multidisciplinary Optimization, 2015, 51(1): 99–112

9. Hamdia K M, Msekh M A, Silani M, Vu-Bac N, Zhuang X, Nguyen-Thoi T, Rabczuk T. Uncertainty quantification of the fracture properties of polymeric nanocomposites based on phase field modeling. Composite Structures, 2015, 133: 1177–1190

10. Msekh M A, Silani M, Jamshidian M, Areias P, Zhuang X, Zi G, He P, Rabczuk T. Predictions of J integral and tensile strength of clay/epoxy nanocomposites material using phase field model. Composites. Part B, Engineering, 2016, 93: 97–114

11. Silani M, Talebi H, Hamouda A M, Rabczuk T. Nonlocal damage modelling in clay/epoxy nanocomposites using a multiscale approach. Journal of Computational Science, 2016, 15: 18–23

12. Vu-Bac N, Rafiee R, Zhuang X, Lahmer T, Rabczuk T. Uncertainty quantification for multiscale modeling of polymer nanocomposites with correlated parameters. Composites. Part B, Engineering, 2015, 68: 446–464

13. Vu-Bac N, Lahmer T, Zhang Y, Zhuang X, Rabczuk T. Stochastic predictions of interfacial characteristic of polymeric nanocomposites (PNCs). Composites. Part B, Engineering, 2014, 59: 80–95

14. Vu-Bac N, Silani M, Lahmer T, Zhuang X, Rabczuk T. A unified framework for stochastic predictions of mechanical properties of

polymeric nanocomposites. Computational Materials Science, 2015, 96: 520–535

15. Ghasemi H, Rafiee R, Zhuang X, Muthu J, Rabczuk T. Uncertainties propagation in metamodel-based probabilistic optimization of CNT/polymer composite structure using stochastic multi-scale modeling. Computational Materials Science, 2014, 85: 295–305

16. Shen H S. Nonlinear bending of functionally graded carbon nanotube-reinforced composite plates in thermal environments. Composite Structures, 2009, 91(1): 9–19

17. Ansari R, Faghih Shojaei M, Mohammadi V, Gholami R, Sadeghi F. Nonlinear forced vibration analysis of functionally graded carbon nanotube-reinforced composite Timoshenko beams. Composite Structures, 2014, 113: 316–327

18. Zhang L, Lei Z, Liew K. Free vibration analysis of FG-CNT reinforced composite straight-sided quadrilateral plates resting on elastic foundations using the IMLS-Ritz method. Journal of Vibration and Control, 2017, 23(6): 1026–1043

19. Lei Z X, Zhang L W, Liew K M. Vibration of FG-CNT reinforced composite thick quadrilateral plates resting on Pasternak foundations. Engineering Analysis with Boundary Elements, 2016, 64: 1–11

20. Mirzaei M, Kiani Y. Nonlinear free vibration of temperature-dependent sandwich beams with carbon nanotube-reinforced face sheets. Acta Mechanica, 2016, 227(7): 1869–1884

21. Kiani Y. Free vibration of FG-CNT reinforced composite skew plates. Aerospace Science and Technology, 2016, 58: 178–188

22. Wu H, Kitipornchai S, Yang J. Free vibration and buckling analysis of sandwich beams with functionally graded carbon nanotube-reinforced composite face sheets. International Journal of Structural Stability and Dynamics, 2015, 15(7): 1540011

23. Wu H L, Yang J, Kitipornchai S. Nonlinear vibration of functionally graded carbon nanotube-reinforced composite beams with geometric imperfections. Composites. Part B, Engineering, 2016, 90: 86–96

24. Kiani Y. Shear buckling of FG-CNT reinforced composite plates using Chebyshev-Ritz method. Composites. Part B, Engineering, 2016, 105: 176–187

25. Mirzaei M, Kiani Y. Thermal buckling of temperature dependent FG-CNT reinforced composite plates. Meccanica, 2016, 51(9): 2185–2201

26. Kiani Y. Thermal post-buckling of FG-CNT reinforced composite plates. Composite Structures, 2017, 159: 299–306

27. Rafiee M, Yang J, Kitipornchai S. Large amplitude vibration of carbon nanotube reinforced functionally graded composite beams with piezoelectric layers. Composite Structures, 2013, 96: 716–725

28. Kiani Y. Free vibration of functionally graded carbon nanotube reinforced composite plates integrated with piezoelectric layers. Computers & Mathematics with Applications (Oxford, England), 2016, 72(9): 2433–2449

29. Alibeigloo A. Free vibration analysis of functionally graded carbon nanotube-reinforced composite cylindrical panel embedded in piezoelectric layers by using theory of elasticity. European Journal of Mechanics. A, Solids, 2014, 44: 104–115

30. Malekzadeh P, Shojaee M. Buckling analysis of quadrilateral laminated plates with carbon nanotubes reinforced composite layers. Thin-walled Structures, 2013, 71: 108–118

31. Malekzadeh P, Zarei A R. Free vibration of quadrilateral laminated plates with carbon nanotube reinforced composite layers. Thin-walled Structures, 2014, 82: 221–232

32. Lei Z X, Zhang L W, Liew K M. Free vibration analysis of laminated FG-CNT reinforced composite rectangular plates using the kp-Ritz method. Composite Structures, 2015, 127: 245–259

33. Lei Z X, Zhang L W, Liew K M. Buckling analysis of CNT reinforced functionally graded laminated composite plates. Composite Structures, 2016, 152: 62–73

34. Lin F, Xiang Y. Vibration of carbon nanotube reinforced composite beams based on the first and third order beam theories. Applied Mathematical Modelling, 2014, 38(15–16): 3741–3754

35. Liew K M, Lei Z X, Zhang L W. Mechanical analysis of functionally graded carbon nanotube reinforced composites: A review. Composite Structures, 2015, 120: 90–97

36. Qu Y, Long X, Li H, Meng G. A variational formulation for dynamic analysis of composite laminated beams based on a general higher-order shear deformation theory. Composite Structures, 2013, 102: 175–192

37. Vo-Duy T, Duong-Gia D, Ho-Huu V, Vu-Do H C, Nguyen-Thoi T. Multi-objective optimization of laminated composite beam structures using NSGA-II algorithm. Composite Structures, 2017, 168: 498–509

38. Vo-Duy T, Ho-Huu V, Do-Thi T D, Dang-Trung H, Nguyen-Thoi T. A global numerical approach for lightweight design optimization of laminated composite plates subjected to frequency constraints. Composite Structures, 2017, 159: 646–655

39. Ho-Huu V, Do-Thi T D, Dang-Trung H, Vo-Duy T, Nguyen-Thoi T. Optimization of laminated composite plates for maximizing buckling load using improved differential evolution and smoothed finite element method. Composite Structures, 2016, 146: 132–147

40. Vo-Duy T, Nguyen-Minh N, Dang-Trung H, Tran-Viet A, Nguyen-Thoi T. Damage assessment of laminated composite beam structures using damage locating vector (DLV) method. Frontiers of Structural and Civil Engineering, 2015, 9(4): 457–465

41. Dinh-Cong D, Vo-Duy T, Nguyen-Minh N, Ho-Huu V, Nguyen-Thoi T. A two-stage assessment method using damage locating vector method and differential evolution algorithm for damage identification of cross-ply laminated composite beams. Advances in Structural Engineering, 2017, 20(12): 1807–1827

42. Vo-Duy T, Ho-Huu V, Dang-Trung H, Nguyen-Thoi T. A two-step approach for damage detection in laminated composite structures using modal strain energy method and an improved differential evolution algorithm. Composite Structures, 2016, 147: 42–53

43. Chandrashekhara K, Krishnamurthy K, Roy S. Free vibration of composite beams including rotary inertia and shear deformation. Composite Structures, 1990, 14(4): 269–279

44. Khdeir A A, Reddy J N. Free vibration of cross-ply laminated beams with arbitrary boundary conditions. International Journal of Engineering Science, 1994, 32(12): 1971–1980

45. Kameswara Rao M, Desai Y M, Chitnis M R. Free vibrations of laminated beams using mixed theory. Composite Structures, 2001, 52(2): 149–160

46. Ramtekkar G S, Desai Y M, Shah A H. Natural vibrations of laminated composite beams by using mixed finite element modelling. Journal of Sound and Vibration, 2002, 257(4): 635–651

47. Kisa M. Free vibration analysis of a cantilever composite beam with multiple cracks. Composites Science and Technology, 2004, 64(9): 1391–1402

48. Li J, Huo Q, Li X, Kong X, Wu W. Vibration analyses of laminated composite beams using refined higher-order shear deformation theory. International Journal of Mechanics and Materials in Design, 2014, 10(1): 43–52

49. Mantari J L, Canales F G. Free vibration and buckling of laminated beams via hybrid Ritz solution for various penalized boundary conditions. Composite Structures, 2016, 152: 306–315

50. Nguyen T K, Nguyen N D, Vo T P, Thai H T. Trigonometric-series solution for analysis of laminated composite beams. Composite Structures, 2017, 160: 142–151

51. Sayyad A S, Ghugal Y M, Naik N S. Bending analysis of laminated composite and sandwich beams according to refined trigonometric beam theory. Curved and Layered Structures, 2015, 2(1): 279–289

52. Jun L, Hongxing H, Rongying S. Dynamic finite element method for generally laminated composite beams. International Journal of Mechanical Sciences, 2008, 50(3): 466–480

53. Shi G, Lam K Y. Finite element vibration analysis of composite beams based on higher-order beam theory. Journal of Sound and Vibration, 1999, 219(4): 707–721

54. Reddy J N, Khdeir A. Buckling and vibration of laminated composite plates using various plate theories. AIAA Journal, 1989, 27(12): 1808–1817

55. Natarajan S, Chakraborty S, Thangavel M, Bordas S, Rabczuk T. Size-dependent free flexural vibration behavior of functionally graded nanoplates. Computational Materials Science, 2012, 65: 74–80

56. Amiri F, Millán D, Shen Y, Rabczuk T, Arroyo M. Phase-field modeling of fracture in linear thin shells. Theoretical and Applied Fracture Mechanics, 2014, 69: 102–109

57. Nguyen-Thanh N, Zhou K, Zhuang X, Areias P, Nguyen-Xuan H, Bazilevs Y, Rabczuk T. Isogeometric analysis of large-deformation thin shells using RHT-splines for multiple-patch coupling. Computer Methods in Applied Mechanics and Engineering, 2017, 316: 1157–1178

58. Areias P, Rabczuk T, Msekh M A. Phase-field analysis of finite-strain plates and shells including element subdivision. Computer Methods in Applied Mechanics and Engineering, 2016, 312: 322–350

59. Nguyen-Thanh N, Kiendl J, Nguyen-Xuan H, Wüchner R, Bletzinger K U, Bazilevs Y, Rabczuk T. Rotation free isogeometric thin shell analysis using PHT-splines. Computer Methods in Applied Mechanics and Engineering, 2011, 200(47–48): 3410–3424

60. Rabczuk T, Gracie R, Song J H, Belytschko T. Immersed particle method for fluid-structure interaction. International Journal for Numerical Methods in Engineering, 2010, 81(1): 48–71

61. Areias P, Rabczuk T. Finite strain fracture of plates and shells with configurational forces and edge rotations. International Journal for Numerical Methods in Engineering, 2013, 94(12): 1099–1122

62. Chau-Dinh T, Zi G, Lee P S, Rabczuk T, Song J H. Phantom-node method for shell models with arbitrary cracks. Computers & Structures, 2012, 92–93: 242–256

63. Nguyen-Thanh N, Valizadeh N, Nguyen M N, Nguyen-Xuan H, Zhuang X, Areias P, Zi G, Bazilevs Y, De Lorenzis L, Rabczuk T. An extended isogeometric thin shell analysis based on Kirchhoff-Love theory. Computer Methods in Applied Mechanics and Engineering, 2015, 284: 265–291

64. Rabczuk T, Areias P M A, Belytschko T. A meshfree thin shell method for non-linear dynamic fracture. International Journal for Numerical Methods in Engineering, 2007, 72(5): 524–548

65. Tan P, Nguyen-Thanh N, Zhou K. Extended isogeometric analysis based on Bézier extraction for an FGM plate by using the two-variable refined plate theory. Theoretical and Applied Fracture Mechanics, 2017, 89: 127–138

66. Kruse R, Nguyen-Thanh N, De Lorenzis L, Hughes T J R. Isogeometric collocation for large deformation elasticity and frictional contact problems. Computer Methods in Applied Mechanics and Engineering, 2015, 296: 73–112

67. Thai C H, Nguyen-Xuan H, Nguyen-Thanh N, Le T H, Nguyen-Thoi T, Rabczuk T. Static, free vibration, and buckling analysis of laminated composite Reissner-Mindlin plates using NURBS-based isogeometric approach. International Journal for Numerical Methods in Engineering, 2012, 91(6): 571–603

68. Huang J, Nguyen-Thanh N, Zhou K. Extended isogeometric analysis based on Bézier extraction for the buckling analysis of Mindlin-Reissner plates. Acta Mechanica, 2017, 228(9): 3077–3093

69. Nguyen-Thanh N, Zhou K. Extended isogeometric analysis based on PHT-splines for crack propagation near inclusions. International Journal for Numerical Methods in Engineering, 2017, 112(12): 1777–1800

70. Zienkiewicz O C, Taylor R L, Zhu J Z. The Finite Element Method: Its Basis and Fundamentals. 7th ed. Oxford: Butterworth-Heinemann, 2013

71. Hughes T J R, Cottrell J A, Bazilevs Y. Isogeometric analysis: CAD, finite elements, NURBS, exact geometry and mesh refinement. Computer Methods in Applied Mechanics and Engineering, 2005, 194(39–41): 4135–4195

72. Zienkiewicz O C, Taylor R L, Too J M. Reduced integration technique in general analysis of plates and shells. International Journal for Numerical Methods in Engineering, 1971, 3(2): 275–290

73. Prathap G, Bhashyam G R. Reduced integration and the shear-flexible beam element. International Journal for Numerical Methods in Engineering, 1982, 18(2): 195–210